BNL-223031-2022-JAAM

Radiation-induced long-lived transients and metal particle formation in solid KCI-MgC12 mixtures

A. Ramos-Ballesteros, J. Wishart

To be published in "The Journal of Physical Chemistry"

May 2022

Chemistry Department

Brookhaven National Laboratory

U.S. Department of Energy

USDOE Office of Science (SC), Basic Energy Sciences (BES) (SC-22)

DISCLAIMER

Radiation-Induced Long-Lived Transients and Metal Particle Formation in Solid KCl-$MgCl_2$ Mixtures

Alejandro Ramos-Ballesteros[1], Ruchi Gakhar[2], Michael E. Woods[2], Gregory P. Horne[3], Kazuhiro Iwamatsu[4], James F. Wishart[4], Simon M. Pimblott[3], and Jay A. LaVerne[1,5].*

[1]Notre Dame Radiation Laboratory, University of Notre Dame, Notre Dame, Indiana 46556

[2]Pyrochemistry and Molten Salt Systems Department, Idaho National Laboratory, Idaho Falls, ID 83415

[3]Center for Radiation Chemistry Research, Idaho National Laboratory, Idaho Falls, ID 83415

[4]Chemistry Division, Brookhaven National Laboratory, Upton, NY 11973

[5]Department of Physics and Astronomy, University of Notre Dame, Notre Dame, Indiana 46556

Corresponding Author

*Email: Jay.A.LaVerne.1@nd.edu

ABSTRACT

The electron paramagnetic resonance (EPR) and diffuse reflectance-optical absorption spectra of room temperature gamma-irradiated KCl-$MgCl_2$ binary solid salt mixtures (98:2 mol% and 2:98 mol%) and the eutectic (68:32 mol%) are reported. Additionally, powder X-ray diffraction of the pristine salts and thermal annealing studies of the irradiated salts were performed to evaluate radiolysis product stability, annihilation, and association in metallic particles. The main long-lived transient species detected in 98:2 mol% KCl-$MgCl_2$ salts were perturbed F-centers, i.e., trapped electrons (e_t^-) in the vicinity of Mg ions (λ_{max} at 561 nm), and the radiolytic reduction of Mg^{2+} to Mg^{+} and Mg^0. Thermal annealing promoted the diffusion of defects to yield polycations (Mg_n^+). On the other hand, irradiation of 2:98 mol% KCl:$MgCl_2$ salts showed the formation of cationic and neutral Mg dimers (Mg_2^+ and Mg_2) and trimers, as well as centers with a rhombic powder pattern apparently consisting of an electron shared between three Mg^{2+} nuclei associated with an anion vacancy (v_a^+- Mg_3^{5+}). Trapped electrons (e_t^-) (F-centers) were not observed in the irradiated eutectic mixture, instead, Mg_2, Mg^0 and Cl_3^- were observed. The higher temperature for thermal ionization of radiation-reduced Mg species decreased the extent of electron recombination reactions and the disproportionation of Cl_3^- compared to the pure KCl, instead, enhanced aggregation of Mg into larger metallic microstructures (metallic particles) was observed.

INTRODUCTION

Concerns about climate change are accelerating the development of competitive sustainable energy production technologies. Among these concepts, molten salt reactors (MSRs) have the

characteristics to be a game-changing technology that positions nuclear energy (along with wind, hydropower, and solar) as a viable path towards decarbonization of the energy sector. The use of molten salts as a coolant and as a matrix for liquid-fueled reactors enables higher operating temperatures (600-800°C) while maintaining safer, nearly atmospheric, operating pressures. As an emerging technology, MSRs face several challenges to effective deployment, for example, the need for strict control of fissile fuel, decay product, and fission product chemistry in the core.[1] Accumulation of deleterious products will affect the neutron economy, redox environment, and consequently, the integrity and functionality of the reactor. For this reason, and in the search for suitable candidates for employment as a coolant in MSR, a thermophysical and thermochemical properties assessment, as well as a thorough understanding of the radiation-induced reactivity due to the exposure to radiation fields on the salts, are required. One of the candidates that has attracted attention due to its high relative solubility, boiling point, specific heat, heat transfer, viscosity, redox potential, and stability, is the KCl-$MgCl_2$ mixture, with proved characteristics to function as a heat transfer fluid for solar energy storage systems. Because of this, studies related to physicochemical and thermodynamic properties of the eutectic mixture have been reported,[2-5] but large knowledge gaps must be addressed in the radiation chemistry area.

Electron pulse radiolysis studies have provided fundamental kinetic data regarding primary short-lived transients (<10^{-6}), such as solvated electrons (e_s^-), and Cl_2^-;[6] however, an interesting approach to assess speciation of the primary and secondary radiolysis products is through the interrogation of solid-state radiolysis. Under a limited diffusion environment, the radiation-induced transients eventually are trapped in the crystal lattice, with a characteristic stability that facilitates its analysis under milder conditions. Although diffusion and reactivity of radiation-induced intermediates in alkali halides differ between the molten and solid phases, experimental

evidence has proven that primary transients induced by gamma radiation are essentially the same in both phases,[7] moreover, the evolution of primary radicals to secondary products observed in the solid state (different to recombination), is likely to occur to some extent in the melt, due to the existing intermediate-range order through combinations of short-range interactions when mixtures of different salts are used.[8] Solid-state radiolysis studies do not provide information of the final products or their kinetics, but indicate the initial radicals formed and their probable association in products different to recombination. Much more work is necessary, but through different approaches such as the present study, mechanistic information is provided that potentially helps in the construction of predictive models for MSRs.

A general scheme of the progression that succeed the interaction of the ionizing radiation on alkali chlorides is as follows: initially-produced primary species (excitons and e^--$Cl^\cdot$ pairs) eventually recombine or get isolated as trapped electrons (e_t^-) (F-centers), and Cl_2^- (H- and V_k-centers). As the density of primary transients increases and diffusion occurs, nucleation starts yielding secondaries such as Cl_3^-, Cl_2, and metallic clusters, which ultimate end up as colloidal centers and dislocation loops (polychlorides) at higher doses and temperatures.[9] The yield and reactions of transients are determined not only by the characteristics of the salt, type of radiation, total radiation dose, dose rate, and temperature, but also by the presence of impurities or dopants. Exogeneous cations can act as electron traps or perturb the radiation-induced defects in the matrix due to their ionization potential. The effect of different low second-ionization-potential cations (<12 eV); such as Ca^{2+}, Sr^{2+}, Ba^{2+}, and rare earths (Eu^{2+}, Sm^{2+}, Yb^{2+}); and high second-ionization-potential dopants (>16 eV); including Cd^{2+}, Pb^{2+} Zn^{2+}, Bi^{2+}, and Mn^{2+}; were summarized by Radhakrishna,[10] reporting a prevailing radiolytic reduction to monovalent or zerovalent for the second group, meanwhile low second-ionization-potential metals only showed perturbed F-centers

after post irradiation heating (or optical bleaching) where the electrons released from F-centers are trapped in shallow sites close to the dopant. With these two scenarios in mind, studies of Mg^{2+}-doped salts with an "intermediate" second ionization potential (I=15.03 eV) are of particular interest. Sootha & Singh[11] performed optical absorption, conductivity, and EPR studies on additively colored KCl crystals doped with Mg^{2+}, reporting the absence of other paramagnetic centers besides F-centers, and observing Mg metal via an absorption band at 272 nm. For their part, Watterich & Raksányi[12] assigned a narrow resonance line (2.6 mT, g= 2.002) to Mg^{+}, and correlated to a 327 nm absorbance in room temperature X-irradiated KCl:Mg doped crystals with and without prior annealing. Damm et al.[13] focused on the effect of the dopant in the initial stage of *F*-center formation/suppression through optical absorption and thermoluminescence of X- and gamma-irradiated KCl:$MgCl_2$ (~5 mol ppm) crystals at room temperature. The authors correlate diffusion coefficients with aggregate production as the explanation for the evident suppression in the presence of Mg^{2+} in comparison with Pb^{2+} as a dopant.

The improved resolution of current generation EPR spectrometers and diffuse reflectance probes make it possible to deepen what was reported by Damm and collaborators, not only concerning the F-centers but also with respect to the radiolytic reduction of Mg^{2+} and the formation of polyhalides, through modifying the proportion of the cations and their effect on the crystalline structure. Here, the identification and stability of gamma radiation-induced (up to 100 kGy) long-lived transients in previously fused KCl-$MgCl_2$ powders of varying compositions are reported for the eutectic, 2:98 mol% KCl, and 98:2 mol% KCl. Low dose rate gamma radiation generates homogeneous and isolated defects in the crystal without knock-on displacements inherent to heavy particle radiations, facilitating their identification. Transient analysis was performed post-irradiation by diffuse reflectance-optical absorption and electron paramagnetic resonance (EPR)

techniques at room temperature (295 K). When combined with previous work on neat KCl and $MgCl_2$ salts,[14] the presented results help to visualize how speciation changes when going from a monovalent to a divalent matrix, as well as clusters, colloids, and polyhalide formation, and the effect of asymmetric environments of mixed cations on trapped electrons (unlike the periodicity in pure KCl or $MgCl_2$) without signal saturation due to the low dose rates used.

METHODS

All salt mixture sample preparations were performed at Idaho National Laboratory (INL) using an argon atmosphere glovebox (VTI, Model number VTISS1-1809-0100) operated at less than 1 ppm H_2O and O_2. $MgCl_2$ was obtained commercially and purified via fractional distillation at Oak Ridge National Laboratory (ORNL), as previously described.[15] Anhydrous KCl beads (Sigma-Aldrich, 99.999% trace metal basis) were used without further purification. KCl-$MgCl_2$ mixtures were prepared by weighing powdered, distilled $MgCl_2$ and KCl beads in the required proportions using a Mettler-Toledo balance (Model number TLE204E, precision 0.8 mg) in a minimum of 3 g batches. These were loaded into a glassy carbon crucible (GAK1, 8 mL Sigradur tapered crucible, HTW Germany) and baked for six hours above the liquidus temperature (600°C for the eutectic mixture [68:32 mol%, mass ratio 56.6-43.4%] and 770°C for the 98:2 and 2:98 mol% mixtures). Prior to use, the glassy carbon crucibles were cleaned with HPLC-grade isopropanol (99.9% purity, Sigma-Aldrich) and baked at 700°C for 3 hours in an argon atmosphere. After cooling to the solid state, these mixtures were then crushed to a fine powder using an agate mortar and pestle, loaded into quartz EPR tubes (Suprasil® silica EPR tubes) and flame sealed under an argon atmosphere.

The salt loaded EPR tubes were then irradiated at the Notre Dame Radiation Laboratory using Shepherd 109 Cobalt-60 Gamma Irradiator at ~6.9 Gy min^{-1} up to 100 kGy @ 295 K. Irradiation dosimetry was performed using the Fricke dosimeter[16] and allowance made for the decay of cobalt-60 (^{60}Co, $\tau_{1/2}$ = 5.27 years, $E_{\gamma 1}$ = 1.17 MeV and $E_{\gamma 2}$ =1.33 MeV). No adjustment was made for differences in electron density as quantitative analysis was not performed. Once a desired dose was achieved, post-irradiation diffuse reflectance optical absorption spectroscopy and electron paramagnetic resonance (EPR) were used to interrogate samples.

For diffuse reflectance optical absorption spectroscopy, an Ocean Optics R400-7-Vis/NIR reflection probe (six illumination and one read fibers), a Flame-S-UV-Vis (Ocean optics) spectrophotometer (200 to 800 nm) and Teflon reference, and an Ocean Optics DH-2000-BAL (deuterium-halogen) light source was used in conjunction with a bespoke 3D-printed sample holder, fabricated to attain a fixed angle of 135° with respect to the detection probe. To minimize bleaching, six scans at minimum acquisition time of 1200 ms was used for data collection. Only pseudo absorbance spectra are presented here, as obtained by Kubelka-Munk data treatment.[17] For simplicity, absorption is given in k/s units, which correspond to the quotient between absorption and scattering coefficients.

Thermal annealing of radiation defects provided information on defect annihilation and metal ion/particle coalescence. Two temperature profiles were employed: (i) ~50 K increments from ambient to 440 K (annihilation temperature for the Cl_3^-), with diffuse reflectance spectra taken at each temperature interval; and (ii) a constant temperature of 440 K with data taken at different time intervals. EPR spectra, using a Bruker EMX spectrometer, were obtained in continuous mode, with five scans from 300-400 mT at X-band frequency (9.8 GHz)at 30 dB attenuation and 0.2 mW power.

Samples for X-ray diffraction (XRD) were loaded into an airtight specimen holder (Bruker A100B33) and the phase compositional data was obtained using a Bruker D8 Advance (Germany) with Cu Kα radiation of 1.54060 Angstrom wavelength at Idaho National Laboratory (INL).

RESULTS

The objective of using stoichiometric solid solutions instead of dissolving K or Mg metal, lies in simulating mixed salt systems that may be good candidates as coolants in MSR's. Therefore, to simulate the internal arrangement of the liquid phase (although with higher coordination), and detect radiolytic reductions and possible associations of metals exclusively induced by the radiation, precipitation of the minority phase in the pristine salt must be avoided. In the powder diffractograms shown in Figure S1, the expected layer contraction for the 98:2 mol% KCl-$MgCl_2$ mixture, due to the smaller size of Mg, was observed. Further, the presence of the $KMgCl_3$ phase in crystals of $MgCl_2$ with KCl at 2 mol% was also seen. There were no significant signal contributions from metal oxide or hydroxide species, which are easily formed by the hygroscopic $MgCl_2$ and can lead to false defects in irradiated crystals.

KCl:$MgCl_2$ (98:2 mol%)

The characteristic room-temperature EPR spectrum of irradiated pure KCl shows a broad, symmetric band (g = 1.9953), with 4.94 ± 0.6 mT linewidth,[14] which parabolically increases in amplitude with absorbed gamma dose without reaching saturation below 100 kGy, Figure S2. The observed F-center powder pattern corresponds to the envelope of 703 lines due to the interaction of one trapped electron in an anion vacancy surrounded by K^+ ions ($I = {}^3/_2$). On the other hand, the EPR spectra of KCl doped with $MgCl_2$ (2 mol%) (Figure 1) shows a more complex set of dose-dependent resonance lines with slightly different magnetic susceptibilities. Figure 1a details the

deconvoluted curves contributing to the central line: F-centers (pure and perturbed), Mg^{+}, and Mg^{0}. A small presence of Mg cluster defects, composed of a set of sharp lines centered at g = 1.9787 and a series of sextets (A = 10.4 mT, lwpp 1.65 mT) induced by the hyperfine interaction from ^{25}Mg (I = 5/2, 10% abundance), were also detected in the pristine samples.[18-19] Through low-power microwave spectra acquisition (0.2 μW) it was possible to resolve the set of lines at g = 1.9787 revealing a sextet (A = 0.14 mT). The collapse of the hyperfine splitting (hfs) is evidence of Mg^{+} being present in nonregular lattice sites, instead, located in interstitials next to K^{+}. This displacement is possible if the association of vacancies with Mg in K_2MgCl_4 crystallites is considered. The sextets are initially insensitive to absorbed gamma dose up to 20 kGy, after which their intensity decreased, albeit still present after 100 kGy.

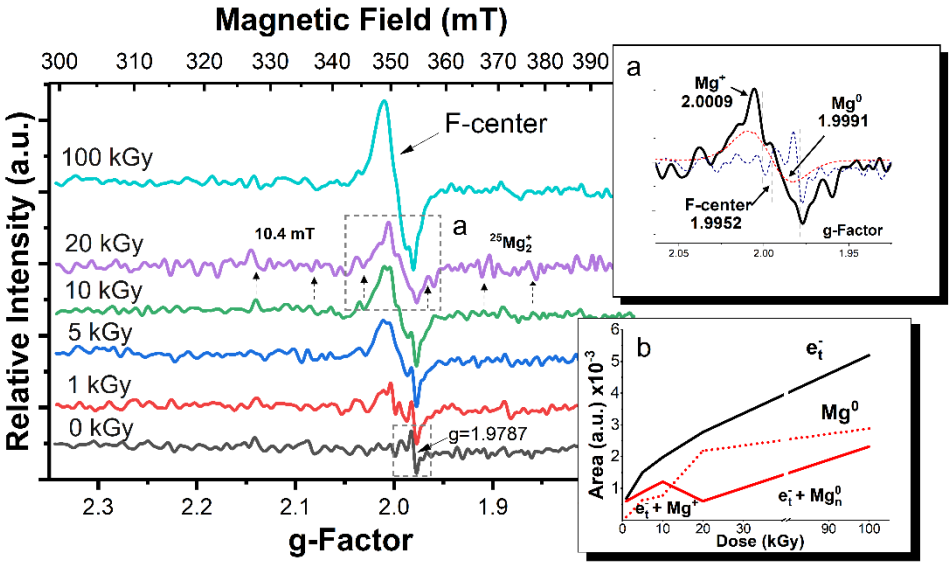

Figure 1. EPR spectra of 98:2 mol% $KCl:MgCl_2$ powders irradiated up to 100 kGy absorbed gamma dose at 295 K. Inset depicts: (a) deconvolution of the central line, with the contribution of F-centers, Mg atoms, and Mg^{+}; and (b) area under the curve for the main EPR resonance line

(g≈1.99) of KCl (black line)[14] and 98:2 mol% KCl:$MgCl_2$ (red line), red dotted line depicts an approximation to the Mg^0 production.

The observed resonance spectra can be summarized as follows: (i) F-center formation (g = 1.9952) occurs even at low absorbed doses despite the presence of an effective electron scavenger such as Mg^{2+}; (ii) the reduction of $Mg^{2+} + e^- \longrightarrow Mg^+$ at g = 2.0009 (lwpp = 0.9 mT) is always present, but is only readily distinguishable in the 1 kGy spectrum, because at higher absorbed doses there is overlap with the broad resonance line of the F-centers; and (iii) a second electron trapping produces zero-valent Mg ($Mg^+ + e^- \rightleftarrows Mg^0$) that is diamagnetic and thus EPR silent; however, coalescence of metal atoms is observable after 10 kGy (g = 1.9991).

F-centers are symmetrical by nature; thus, the asymmetry of the resonance line is indicative of other paramagnetic centers overlapping. The asymmetry parameter (A/B), defined as the quotient of the max/min of the derivative of the absorbed power (dP/dH), differs from the pure KCl (Figure S3), reaching a highest value after 10 kGy of absorbed dose where apparently Mg^+ reaches max equilibrium concentration, to later decrease due to double reduction to the zero-valent state. The presence of Mg^{2+} also modifies the characteristic KCl EPR spectrum's amplitude, mainly dominated for F-centers (Figure S2). A quenched and reduced intensity of the F-center resonance line shows the predominant radiolytic reduction of the divalent at doses below 20 kGy; besides, a shift in the overlapped absorption band (Table 1) is evidence of perturbation or distortion of the isotropic trapped electron.[10] The intensity is schematized in Figure 2b, where the expected near-parabolic growth of trapped electrons from the pure salt (black line) is only observed in the 98:2 mol% KCl:$MgCl_2$ (red line) after 20 kGy, when apparently most of the Mg^{2+} has been reduced and no longer functions as a scavenger. In the first part of the curve, the local maximum at 10 kGy coincides with the higher asymmetry (Table 1) to later decrease after 20 kGy because of the second

reduction to yield zero-valent. Mg^0 is silent in EPR, but a rough estimate can be obtained through comparison of the area under the curve of the resonance line between the pure and doped salts. Since the concentration of Cl_3^- is similar in both (as seen later), it follows that the number of e^--h^+ pairs induced by radiation should not be very different; therefore, the difference between areas under the curve for both salts indicate the number of electrons trapped to generate Mg^0 (red dotted line), although is important to mention the contribution below 10 kGy from Mg^+ to the resonance. The increase in magnetic susceptibility between 20 and 100 kGy for the Mg^0 estimated curve is around 32%, which is probably due to the formation of metallic particles (Mg_n^0). The contribution to the magnetic susceptibility of the itinerant electrons on the surface of metallic particles is less than isolated metal atoms.[20]

The absorption spectra for the irradiated 98:2 mol% KCl:$MgCl_2$ salts (Figure 2) showed the characteristic Cl_3^- bands (234 nm/5.3 eV and 260 nm/4.77 eV), a broad band at 561 nm/2.21 eV for trapped electrons in anion vacancies perturbed by having Mg in the vicinity (perturbed F-centers), low intensity signals associated with Mg around 333 nm/3.72 eV (Figure 2a), and the K colloidal bands (F_2 and F_3-bands, 800 nm/1.55 eV and 737 nm/1.68 eV, respectively).

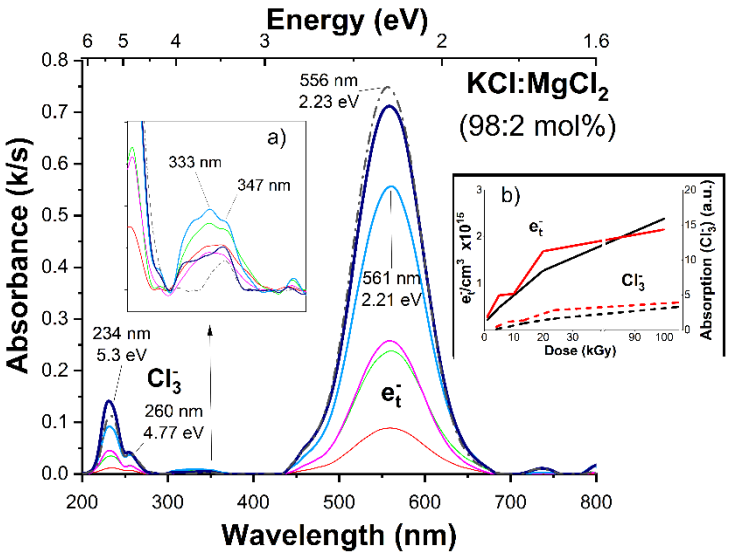

Figure 2. Absorption spectra of irradiated 98:2 mol% KCl:$MgCl_2$ to −1 kGy, −5 kGy, −10 kGy, −20 kGy, −100 kGy, and pure KCl (100 kGy, black dotted line). Spectra obtained through Kubelka-Munk treatment of diffuse reflectance optical absorption, 0 kGy subtraction, and baseline correction. (a) Absorption bands for reduced Mg and (b) increase in density of e_t^- (solid) and Cl_3^- (dotted) in KCl (black lines) and 98:2 mol% KCl:$MgCl_2$ (red lines) irradiated salts. Figure 2b shows the evolution of e_t^- (F-centers) and Cl_3^- for KCl and 98:2 mol% KCl:$MgCl_2$, obtained through the 561 nm and 234 nm absorption bands. The density of trapped electrons (e_t^-/cm^3) (Table 1) was calculated with the Smakula's equation,[21]

$$N(cm^{-3})f=54.1\frac{n}{(n^2+2)^2}\int \alpha(\omega)(cm^{-1})d\omega \quad (1)$$

where n is the refraction index (n = 1.4862 @ 556 nm), α is the max absorption, f is the oscillator strength (f = 0.8 for KCl)[22] and the FWHM (ΔE) in frequency (ω) units (s^{-1}) was estimated with:

$$\Delta\omega = \frac{\Delta E}{\hbar} = \frac{\Delta E}{6.59\times10^{-16}eVs} \quad (2)$$

The peak area is given by the approximation

$$\int \alpha(\omega)d\omega \approx \alpha_{max} \times \Delta\omega \quad (3)$$

while the concentration of Cl_3^- was estimated through the peak area for the 234 nm absorption band (Figure 2b, right axis).

Table 1. Trapped electron density (F-center)* and EPR parameters for the pure and 98:2 mol% KCl:$MgCl_2$ irradiated powders.

Dose (kGy)	**KCl** (e_t^- / cm^3)	**KCl:$MgCl_2$** (e_t^- / cm^3)	**KCl:$MgCl_2$ (g-factor)**	**KCl:$MgCl_2$ (width) (Gauss)**	**Asymmetry parameter (A/B)**
1	2.11 x10^{14}	2.81 x10^{14}	1.9930	64.4	1.23
5	4.78 x10^{14}	7.43 x10^{14}	1.9932	51.1	1.83
10	7.37 x10^{14}	8.74 x10^{14}	1.9941	49.8	1.92
20	1.27 x10^{15}	1.69 x10^{15}	1.9920	51.5	1.70
100	2.38 x10^{15}	2.15 x10^{15}	1.9971	50.6	1.25

* Electron density calculated from the 561 nm band through equation 1.

A three-stage e_t^-/cm^3 curve was observed. An initial fast production (<5 kGy) due to the higher density of available vacancies (cation-vacancy dipoles) induced by the divalent ion in the lattice, followed by a plateau (5-10 kGy) where the equilibrium $Mg^+ + e^- \rightleftarrows Mg^0$ becomes important deaccelerating the F-center production, and a final slower yield limited by the rate of gamma-radiation induced vacancies. Unlike the EPR results, the observed F-centers in the absorption spectra were always generated, and higher than the pure KCl. The proportional relationship between the EPR spectrum integral area and F-center concentration is well known, but apparently the presence of the divalent ions modifies the spin-lattice relaxation time, related with increased width (Table 1), or an equilibrium between F-centers and perturbed F-centers producing spin-exchange facilitated by temperature. In the same way, trapped holes (Cl_3^-) should be formed as

counterpart of the trapped electrons. A typical comparison in alkali halides is a quotient between F-center/Cl_3^- absorption, where change in the slope is related to the presence of impurities and density of intrinsic vacancies (initially present in the crystal). In Ca^{2+} and Sr^{2+}-doped crystals, with lower 2nd ionization potentials (11.87 and 11.03 eV, respectively), the slope for low dose is ~ 3;[23] while in the present study, a slope of 4.65 for 98:2 mol% KCl:$MgCl_2$ (Figure S4) is indicative of a more efficient F-center formation due to the higher amount of free positive vacancies.[24] The absorption spectra also showed ~25% more Cl_3^- in $MgCl_2$-doped salts with respect to pure KCl, supporting the mechanism of Mg^{2+} reduction and F-center formation happening at the same time. The growth rates change from 1.2 x 10^{14} e_t^-/kGy·cm^3 for the initial stage (1-5 kGy), 6.1 x 10^{12} e_t^-/kGy·cm^3 for the equilibrium point (5-10 kGy), 9.1 x 10^{13} e_t^-/kGy·cm^3 within 10–20 kGy range, and finally, the late stage of coloration with the lowest growth of 5.8 x 10^{12} e_t^-/kGy·cm^3.

Two bands with maxima at 314 nm and 333 nm are another manifestation of Mg^{2+} reduction (Figure 2a). The former corresponds to Mg^+,[12] while the latter has been related to Cl_2. Apparently, the presence of Mg^{2+} increases the production of chlorine since it was not detected in the pure crystals (black dotted line). The 347 nm band (also present in pure KCl) probably corresponds to a small amount of Cl_2^- occupying one lattice point (*H*-center) near the divalent cation, since as shown below, it disappears with increasing temperature.

After heating, the 561 nm band (e_t^-) and 234 nm (Cl_3^-) progressively disappeared as expected, and new bands appeared with max absorbance at 412 nm (3.01 eV) and three bands in the 350-400 nm range (Figure 3). These new bands increased in intensity up to 440 K to later bleach after 30 min keeping temperature. According to the absorption behavior of atomic clusters in noble gas matrices reported by McCaffrey,[25] and in doped crystals studied by Voszka,[26] these bands can be

ascribed to the association of Mg metal atoms in charged clusters (polycations) such as Mg_2^+, Mg_3^+ and Mg_4^+.

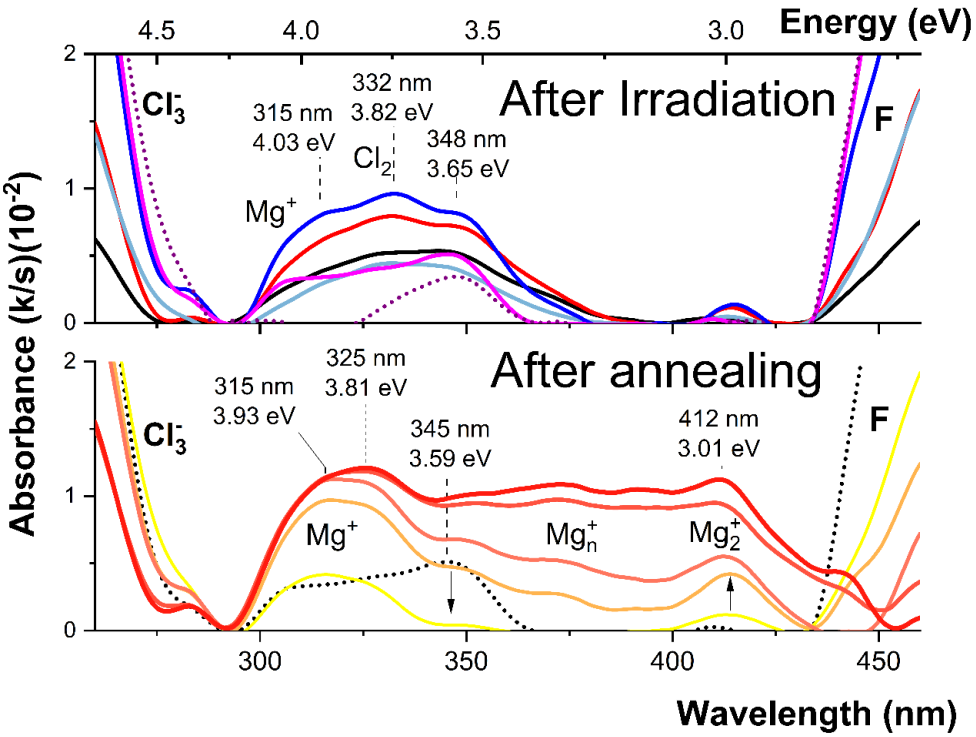

Figure 3. Absorption spectrum for 98:2 mol% KCl:$MgCl_2$ after gamma irradiation and after thermal annealing up to 440 K in the range of Mg metal absorption (250-450 nm). Top: ▬ 1 kGy, ▬ 5 kGy, ▬ 10 kGy, ▬ 20 kGy, ▬ 100 kGy and ···KCl-100 kGy. Bottom: ··· 295 K, ▬ 370 K, ▬ 415 K, ▬ 423 K, ▬ 440 K (20 min) and ▬ 440 K (30 min).

The thermal annealing of the crystals confirmed the composite nature of the 561 nm band. A tail on the long-wavelength side of the F-center band appeared (Figure S5), showing perturbed F-centers due to impurities other than Mg, or due to F-centers in the vicinity of metallic Mg particles.

At low temperatures (<400 K), trapped electrons are released in a pseudo-first order in KCl (Figure S6), recombining with Cl_3^-, or getting trapped again in associated vacancies to form F_2 and

F_3 centers (colloidal particles). For the 98:2 mol% KCl:$MgCl_2$, the decay is almost linear up to 393 K, where apparently the presence Mg metal hinders recombination of trapped electrons and Cl_3^-. Close to 415 K, the density of e_t^- exhibits an increase because of the thermal ionization of Mg^0, releasing electrons to feed the 561 nm band.

KCl:$MgCl_2$ (2:98 mol%)

In a previous work, the long-lived transients induced by gamma radiation in $MgCl_2$ powders were reported, highlighting the radiolytic reduction of magnesium.[14] $MgCl_2$ has a $CdCl_2$ crystal structure ($R\bar{3}m$) with a two-layer laminar arrangement of close-packed chlorine ions per one layer of Mg, with Mg^{2+} ions occupying distorted octahedral interstitials.[27] Unlike a simple substitution of cations when divalent ions are incorporated into KCl matrices, the incorporation of large K^+ ions in $MgCl_2$ distorts the lattice parameter, as well as the volume of the vacancies and interstitial spaces, giving rise to new bands in the absorption and EPR spectrum. Powder diffractions (Figure S1) showed the characteristic structure of chloromagnesite with a series of peaks around $2\theta=36$ due to the presence of K^+, apparently in a $KMgCl_3$ phase.

Figure 4 shows the spectra for the 2:98 mol% KCl:$MgCl_2$ salts irradiated at 1, 5, 10, 20 and 100 kGy absorbed dose. Traces of Mn detected in the pristine sample (sextet with A = 8.46 mT) did not represent a significant interference since its concentration remains in equilibrium throughout irradiations. The gamma irradiated $MgCl_2$ EPR powder pattern has a well-defined axial center ($g_\perp > g_\parallel$) with a Lorentzian $g_\perp = 2.0248$, and a gaussian of less intensity for parallel centers at $g_\parallel = 2.0081$ at room temperature.[14] In a previous work the resonance was assigned to an electron shared between Mg ions as an F-center , but the results obtained here provided more information about the characteristic of this paramagnetic center. The doped salts showed a rhombic powder

pattern with three absorptions at g_1= 2.1338, g_2=2.0233 and g_3= 2.0081; and a second center around g=2.0009, probably associated with Mg^+ as seen in the 98:2 mol% KCl:$MgCl_2$ system.

The inset shows the EPR spectra of pure (blue) and K+-doped $MgCl_2$ (black) after 1 kGy absorbed dose with their respective integral curves. The almost equal intensity of the absorptions (red curve) is evidence of a second center overlapping the $g_{\parallel}$ of the axial center detected in pure $MgCl_2$.

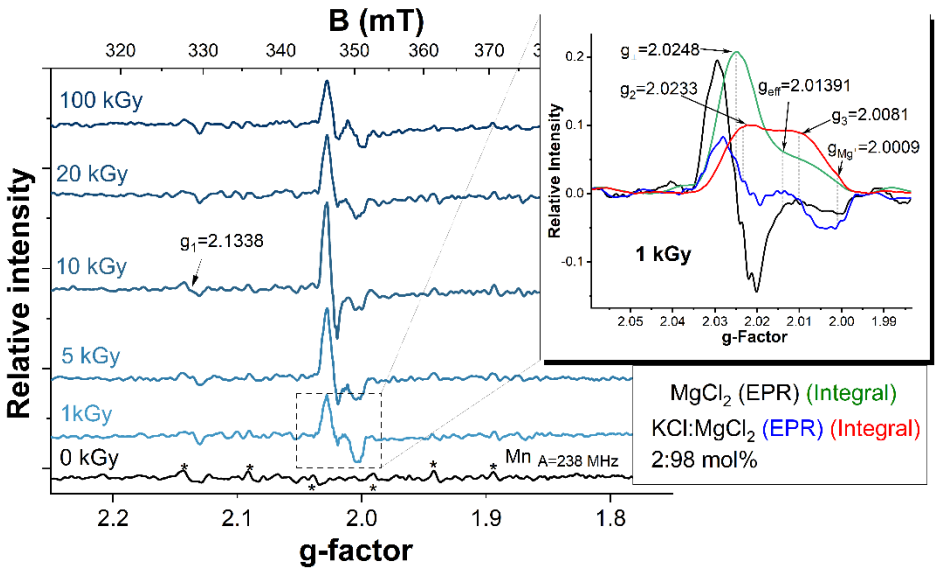

Figure 4. Room temperature EPR spectra for gamma irradiated 2:98 mol% KCl:$MgCl_2$ powders. Inset shows the 1 kGy EPR spectra with corresponding integral curves for $MgCl_2$ and 2:98 mol% KCl:$MgCl_2$.

Figure 5 shows the EPR parameters for both systems, and differences in intensity, asymmetry, linewidth and even g-shift are clearly observed. The main resonance line (g_2), although following a similar trend, decreased by ~32% in intensity with respect to pure salt (Figure 5a). The relative intensity of both signals (g_2 and g_3) should follow a similar growth/decrease pattern if they belong

to the same center, which was not observed for the doped salt where even the intensity of g_3>g_2, confirming the contribution of another paramagnetic center with maximum contribution to line g_3 after 20 kGy absorbed dose. Upon reaching 100 kGy, both peaks again present similar intensities, indicative that the second specie has been consumed, there is delocalization of charge, or the particle size is big enough to produce dispersion of the microwaves (>skin depth δ).

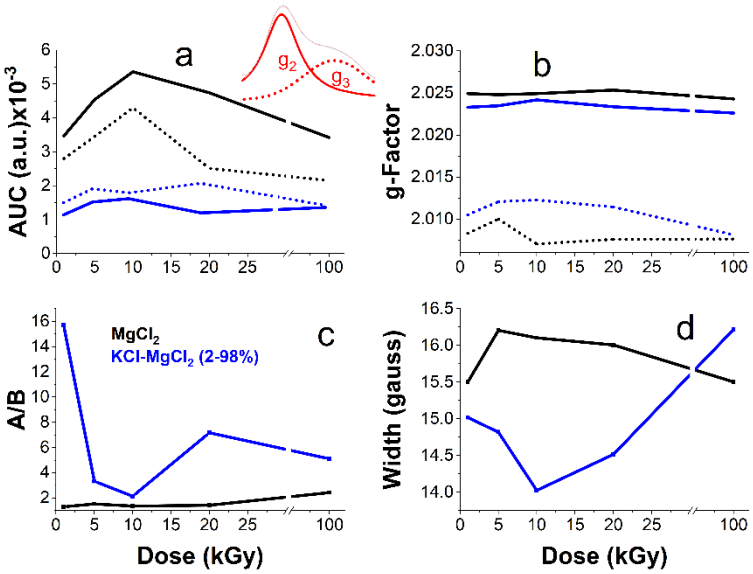

Figure 5. EPR parameters for the gamma irradiated $MgCl_2$ (black) and 2:98 mol% KCl:$MgCl_2$ (blue) salts at room temperature. (a) peak areas (integral curves) and (b) effective g-factor of the two main resonance lines (g_2 and g_3); (c) asymmetry parameter, and (d) peak to peak linewidth for main resonance line (g_2).

The doped spectrum also shows a shift to higher field in the g_2, and a shift to lower field on the g_3 line, correlated to the appearance of the second paramagnetic center (Figure 5b). Despite a small increase after 5 kGy (impurities), the g-factors for $MgCl_2$ kept constant with a mean value of $g_{\perp}$=2.0248 ± 0.0003 and $g_{\parallel}$=2.0081 ± 0.0011 (Δg=0.0167). The KCl-doped $MgCl_2$ salt had a

monotonous g_2= 2.0234 ± 0.0005, but a significant shift for the g_3 with maximum at g = 2.0123 after 10 kGy, and a minimum of g = 2.00891 at 100 kGy, very close to the $g_{\|}$ value for the pure $MgCl_2$. Assuming the latter as g_{eff} for the $g_{\|}$ of the axial center, deconvolutions indicated that the g_{eff} for the new species is located around g_{eff} = 2.0139. The shape of the curve confirms which was stated before, that either the paramagnetic center appears to later disappear by destruction with the dose, or dispersion of the microwaves related to size.

The proximity of the resonance lines makes their evaluation difficult, however the asymmetry parameter (A/B, presented in Figure 5c) of the main resonance line can be taken as an indicator of how the concentrations of both species change with respect to the dose, if saturation has not been reached. A higher asymmetry means greater absorption of the species with g_{eff}= 2.0139, while a lower asymmetry is a greater absorption from the rhombic center with g_2=2.0234. The A/B for $MgCl_2$ (black line) remains at values close to 1.3 up to 20 kGy, afterwards the asymmetry raises to 2.4, because of an increase in metallic particle size. For 2:98 mol% KCl:$MgCl_2$, the greatest asymmetry occurs after only 1 kGy absorbed dose, evidence of an easy formation of the new paramagnetic centers probably for the distorted packing because of the K^+ inclusion (with an ionic radius almost twice that of Mg^{2+}). At the same time, the asymmetry reaches a minimum at 10 kGy that coincides with the maximum formation of axial centers in pure $MgCl_2$, and 20 kGy is the maximum absorption for the species with g_{eff} = 2.0139. Considering the peak areas and the above, it seems that only the rhombic centers increase and decrease in the experimental range presented here, while the other center g = 2.0139 remains in equilibrium until 20 kGy, where it begins to disappear.

The linewidth is directly related to the resistivity scattering processes and spin-orbit coupling, which in turn influence the relaxation time.[20] A narrower line is characteristic of a more localized

electron as seen for the spectrum with least asymmetry and highest concentration of rhombic centers (lwpp = 1.4 mT (Figure 5d)). All the evidence collected suggests that the rhombic center is an electron shared between three Mg^{2+} ions associated to an anion vacancy on top of the cation plane in a cubic closed packed arrangement, Mg_3^{5+}-v_a^+, and the other paramagnetic center apparently corresponds to Mg metal particles with an absorption overlapped with the g_3 of the Mg_3^{5+} clusters. The aggregation of metal atoms is facilitated by the presence of K^+, increasing the specific volume (lattice parameter) and modifying the interstitial spaces. The hyperfine interaction of the electron with three Mg nuclei can be observed in Figure S7, where the splitting induced by ^{25}Mg (I = 5/2, 10 %) produces 6 lines or 11 lines if the center contains one or two of the mentioned isotopes, respectively. Finally, the Mg^+ monovalent line, g = 2.001, was not clearly observed due to the overlap with the parallel component of the Mg_n^+ line, although the association of reduced species is more likely than the presence of isolated ions as observed for 98:2 mol% KCl:$MgCl_2$.

The absorption spectrum (Figure 6) of 2:98 mol% KCl:$MgCl_2$ includes the expected bands from pure $MgCl_2$ plus the appearance of reduced Mg species summarized in the Table 2. The bands attributed to radiolytically-reduced Mg species increase with comparable rate, except for the 260 nm band related to neutral Mg dimers that grows slower. The peak at 233 nm attributed to Cl_3^- reaches a maximum after 10 kGy, to later decay due to aggregation to polyhalides, $(Cl_2)_2$.[28] The 5.8 eV (213 nm) peak, particularly evident at higher dose, confirms the latter. After 100 kGy, the 233 nm band increases contrary to the trend followed at lower doses, probably for the presence of Mg_n (n > 3).

Table 2. Main diffuse reflectance optical absorption peaks detected in irradiated 2:98 mol% KCl-$MgCl_2$ salts

λ	nm	**233**	**260**	**285**	**305**	**366**	**473**
	eV	5.32	4.76	4.35	4.06	3.38	2.62
		Cl_3^-	Mg_2	Mg^0	Mg^+	Mg_2	Mg_3^{5+}-v_a^+
Ref.		29	25	26	12	25	-

The 473 nm band follows the trend shown by the rhombic paramagnetic center (Mg_3^{5+}-v_a^+) at g_2=2.0233. The behavior suggests an increase size of the clusters after 10 kGy to aggregate into larger particles. Other bands detected were Mg_2, Mg^0, Mg^+ and cationic dimers Mg_2^+. Unlike the Mg-doped KCl salt, where only atomic species were detected after irradiation, and association in dimers after thermal annealing; in the K-doped $MgCl_2$ salt the intensity is much higher and the association in trimers was evident at 366 nm.

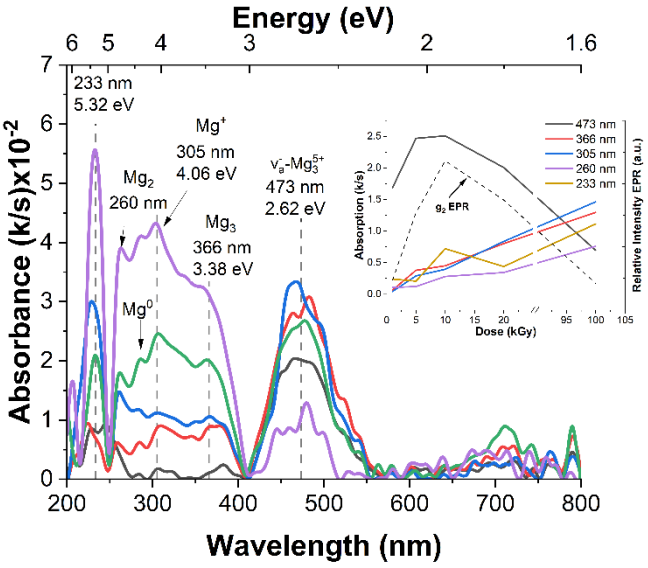

Figure 6. Absorption spectra for 2:98 mol% KCl:$MgCl_2$ irradiated at room temperature up to 100 kGy. Inset shows peak growth for the identified bands. — 1 kGy, — 5 kGy, — 10 kGy, — 20 kGy and — 100 kGy.

The thermal decay profile of the formed centers is similar for the reduced Mg species (Figure S8a), except the band at 366 nm. Apparently, the neutral trimers decay faster by association in larger particles since no increase in the concentration of dimers was observed. The band assigned to Mg_3^{5+} clusters at 471 nm would be expected to decay faster, but apparently the thermal ionization of Mg^+ and unstable polycations continues feeding it up to 440 K. The only signal that continues growing is the 233 nm related to Cl_3^-, which is consistent with the disappearance of polyhalides that break down into smaller molecules. Of the initial radiation-induced species only Mg^0 and Mg^2 showed thermal stability up to 440 K (Figure S8b). The dimers did not show an appreciable change throughout the heating, or the equilibrium of production/destruction was never strongly disturbed. In the final stage, after more than 2 hours at 440 K, equilibrium is reached and the system only exhibits Cl_3^-, Mg^0, dimers, and Mg metallic particles. Only at longer heating times (24 h) a new band appeared (431 nm) for large size particles.

KCl:$MgCl_2$ eutectic (68:32 mol%)

The final system is the eutectic of KCl:$MgCl_2$. The eutectic is not the simple mixture of the components (crystallites), but a crystalline structure with different energy, lattice parameters and coordination. The identified structure (K_2MgCl_4) shows lattice parameters: a=b=c=8.63855, and a unit cell volume = 197.433844 $Å^3$. In the previous systems, the electron trapping in anionic vacancies and the reduction of Mg to monovalent and zerovalent states could be appreciated. Despite sharing components, the proportion and the crystalline structure are what determine the speciation induced by gamma radiation. The irradiated crystals did not show the presence of clusters, nor the presence of Cl_2^- as in the case of $ZnCl_2$ reported in a previous study.[14] The absorption spectra (Figure 7) for irradiated salts only shows two well-resolved peaks with maxima

at 235 nm and 260 nm. The 235 nm signal is related to Cl_3^- bands, while the other is an envelope of bands with maximum absorption at 260 nm and 285 nm corresponding to Mg_2 and Mg^0, respectively. In the central part of the visible region, there is a small absorption apparently insensitive to radiation not possible to identify.

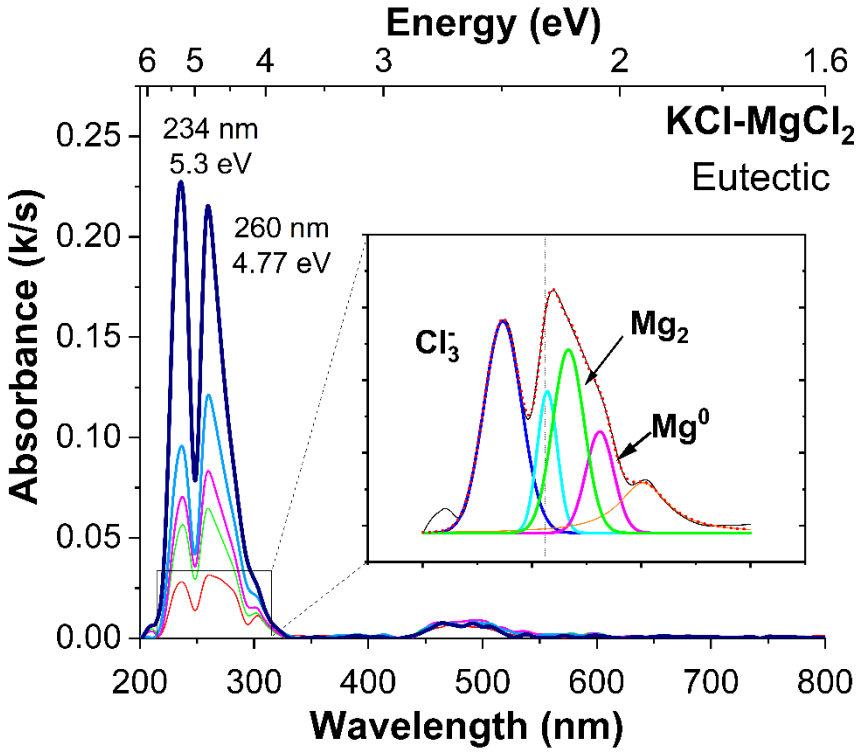

Figure 7. Absorption spectra for KCl:$MgCl_2$ eutectic mixture irradiated at room temperature up to 100 kGy. The inset shows deconvoluted peaks for the 260 nm band. The small turquoise unlabeled band corresponds to Cl_3^- neighboring interstitial ions.

The EPR spectrum of KCl:$MgCl_2$ eutectic (Figure S9) was consistent with the absorption spectrum. No resonance lines were detected at any dose, only traces of Mn (sextet) that intensify after heat treatment (24 h). The thermal annealing (Figure S10) followed a decay profile like 2:98 mol% KCl:$MgCl_2$ salts from the previous section, but with a decay rate for Cl_3^- rather closer to

98:2 mol% KCl:$MgCl_2$ due to the higher percentage of KCl in the mixture. Disproportionation rates of Cl_3^- are shown in Figure S11. The slopes for the 98:2 mol% KCl:$MgCl_2$ salt and the eutectic mixture are similar while the 2:98 mol% KCl:$MgCl_2$ salt is buffered by the stability of magnesium against thermal ionization. The thermal stability of reduced Mg raises the recombination temperature and reduces the rate of disproportionation of Cl_3^-, remaining almost invariable up to 400 K. Even at temperatures above the decomposition (400 K), there will always be metallic particles and Cl_3^-. Another mechanism that inhibits recombination reactions involves metallic colloids in the crystal. The metallic particles act as traps for mobile F-centers after annealing, deactivating them for recombination.

DISCUSSION

In the early 1950's Kantz and Shamovsky began to study the effect of dopants on the radiolytic coloration of alkali halides.[30] Through conductivity measurements in Ag-doped KCl salts, they intuitively proposed the existence of "new centers" that decreased the production of F-centers and gave higher resistance to bleaching. The deeper centers, energetically speaking, function as electron traps, decreasing conductivity and optical absorption. When divalent cations are introduced in solid alkali halides, an imbalance in charges is created only compensated by the generation of new vacancies. The latter has direct consequences in the rate of production of F-centers, which now has two differentiated stages. An initial period (low dose) with a high electron trapping rate due to the higher number of intrinsic vacancies (Figure 2b), followed by a second stage, significantly reduced, where radiation-induced vacancy production regulates the electron trapping ratio. Various models have been proposed for the point defects generated by the inclusion of a divalent ion in a monovalent chloride lattice, with the ion-cation vacancy dipole (I-V) model

as the most supported. The model assumes the association of pairs of cations-anion vacancies in the vicinity of the divalent cation at room temperature.

Summarizing, the inclusion of alkaline earth ions enhances the first stage of F-center formation and suppress its growth at high dose.[23] The mechanism of suppression is not well understood, but it is believed that the migration of metallic particles to dislocation sites inactivates them as hole traps, where Cl_3^- formation is facilitated. Even when the reaction of two Cl_2^- yielding Cl_3^- is not energetically efficient, it turns exothermic in regions of the crystal with more "disorder" like dislocation loops or surfaces.[13, 31] A decrease in Cl_3^- translates into an increased recombination rate, and fewer trapped electrons.

Less clear is the effect of cationic speciation, which is determined by the identity of the ion. Four different effects have been reported for irradiation on monovalent matrices with divalent dopants: a) reduction in the number of I-V dipoles (dopant-vacancy), b) increase in the number of trapped electrons, c) change in the valence state of the doubly-valent ions, and d) modification of the rate of aggregation of dipoles.[32] In simple words, the divalent cations can trap electrons, turning to monovalent cations, or "trap" Cl_2^- (holes) and inhibit Cl_3^- formation. Unlike the rest of the alkaline earth metals, Mg^{2+} acts as an electron trap (scavenger) during irradiation, while the rest of the elements of the second group manage to trap electrons only after thermal bleaching.[23] At room temperature the two alternatives are: cation vacancies pair to anion vacancies (inherent in the crystal) forming a Mg^{2+} ion-pair vacancies dipole, $Mg^{2+}v_cv_a$, which under gamma irradiation is disrupted for the divalent reduction, or e^- trapping in the vacancy pair. If the former happens, the pair of vacancies will be released and available to trap electrons (F-centers) and interstitials, yielding Cl_2^- and eventually Cl_3^-,[24] in addition to Mg^+ or Mg^0, forming dimers and coalescing in bigger particles. If the latter predominates, mainly Z_1-centers will be generated with a small

presence of metallic Mg. The direct trapping of electrons by Mg^{2+} ions seem to fit better with our results; however, there is still the trapping of electrons in vacancies forming F-centers disturbed by the proximity of either Mg^{+} or Mg^{0}. If only the EPR spectrum were observed, it would be thought that almost no F-centers are generated, but the absorption spectrum not only confirms its presence, but in an even higher concentration than in the pure salt. This observation is only understandable if the magnetic susceptibility of electrons trapped in anion vacancies is affected by the presence of Mg in the vicinity (polarization or delocalization of charge).[10] The pure KCl F-center absorbs at 551 nm/2.23 eV (Figure 2, black dotted line), whereas in the mixture 98:2 mol% KCl:$MgCl_2$ the maximum shifts to slightly longer wavelength (561 nm/2.21 eV) giving the perturbed F-center. According to the phase diagram, Mg^{2+} is solidified as a dispersed phase in crystallites with a K_2MgCl_4 structure in a KCl matrix, maintaining octahedral coordination for Mg^{2+}, but higher coordination for K^{+}.[33] Therefore, anion vacancies are expected, bordered either by four K^{+} and two Mg^{2+}, or by five K^{+} and one Mg^{2+} ions, explaining a perturbed F-band from trapped electrons in the vicinity of Mg^{+} ions. The post-irradiation results do not show the clear presence of these centers since the maximum absorption of the F-center band is not far from the value in pure crystals ($\Delta\lambda$ = 5 nm), explicable for slight changes in the lattice parameters for the inclusion of the Mg, but the thermal annealing studies showed a tail in the band at 600-700 nm characteristic of the perturbed F-center. Although the post-irradiation EPR spectra presented a different amplitude and intensity than the F-centers in pure crystals, it cannot be ruled out that said disturbance is due to the reduction of Mg cations and not to the presence of perturbed F-centers.

In addition to the presence of Mg metal particles, the possibility of the existence of colloidal K was not mentioned. Radiation-induced metal atom production is always occurring. Even in pure KCl, the asymmetry parameter increases with dose due to colloidal potassium, $K^{+} + e^{-} \rightarrow K^{0}$

(g=1.9998), but in the presence of Mg with its high ionization potential, the reduction rate decreases. The contribution to the asymmetry from colloidal potassium (K^0) although possible is not significant at room temperature and low dose. The potassium cation reduction and coagulation process F-centers ⇆ colloidal is relevant beyond the second stage of coloration where new anion vacancies are formed, and after the Mg cations present have been heavily reduced. Edmonds *et al*. [34] reported enhancement in colloidal K over post-irradiation annealing above 573 K, with associated absorption bands between 750-850 nm, which were observed here only after 100 kGy absorbed dose.

The radiolytic reduction of Mg was evident in the 3 systems under study. When Mg^{2+} is in low concentration, as in the case of 98:2 mol% KCl:$MgCl_2$, atomic associations occur and the reduction to Mg^+ is significant. The assignments of the g=1.9991 and g=2.0009 lines to Mg metal particles and Mg^+, respectively, agree with the literature, although under different experimental conditions. Watterich & Raksányi[12] found paramagnetic centers (g=2.002 ± 0.001, lwpp=2.6 mT) attributable to Mg^+ in thermal-annealed, X-irradiated KCl:$MgCl_2$ crystals. They correlate the Mg^+ EPR signal with a new UV-Vis band with a maximum at 327 nm that appears after optical bleaching of the F-center band. The new band apparently decreases together with the Cl_3^- at 413 K showing a shift to 317 nm while feeding the F-center vacancy in the same process, which is characteristic of an electron excess center. Based on the above, the band at 315 nm corresponds to Mg^+.[35] The formation of Mg polycations in larger clusters (Mg_3^+ and Mg_4^+) was observed after controlled heating below the decomposition temperature of Cl_3^-. Knight Jr *et al*.[19] found similar values for various Mg^+ polycations in an entirely different environment. They compared experimental data and theoretical simulations of Mg_n^+ clusters (n=2 to 6) condensed at low

temperatures in solid matrices of noble gases, reporting values close to g=2.0017 for dimers in solid Ne.

Different results were observed in the 2:98 mol% KCl:$MgCl_2$ mixture, where the Mg clusters ostensibly increase and the presence of metallic particles and paramagnetic centers (clusters)with rhombic symmetry were detected, apparently due to a trapped electron shared between 3 Mg^{2+} ions. Radiolytic production of clusters of this type has been reported in Ag, using zeolites to control particle size. Gachard et al,[36] identified clusters with absorptions and g-factor similar to those obtained in the present study. The correlation between g-factor and linewidth with the size of metal particles has been a subject of research and little consensus. Sako & Kimura[37] measured Mg particle spectra in media such as hexane and THF, finding a linewidth related to size and medium, but centered around g = 1.997. Bandow *et al*.[38] found a broad signal at g = 2.01 for ultrafine Mg particles under UHV conditions and Millet[39] proposed g-factor shifts in the range between the free electron (g = 2.0023) and bulk Mg (g = 2.061) according to the particle size. It is evident that there is no consensus, but the relationship between particle size and g-factor shift has been proven.[37, 39] Although the particle size cannot be defined, they are undoubtedly present and are contributing to the asymmetry of the band at higher dose.

The eutectic does not behave like a mixture of the two other systems. The specific crystal structure does not allow potential wells deep enough to trap electrons and hold them at room temperature. Instead, electrons ionized by radiation are trapped by Mg^{2+} ions, yielding Mg^0, Mg_2 and Cl_3^-. The formation of metallic Mg particles and thermal ionization buffered by the electronic exchange between clusters was not detected.

The impact of Mg^{2+} concentration on speciation is complicated. Among the main processes determining the electron trapping at room temperature are the efficient formation of Cl_3^- and the

colloidal aggregation.[40-41] Colloidal centers are generally referred for aggregates of F-centers (regions with high density of cations), which can be seen as small metal (fractal) particles of several hundred cations or alkali metal atoms embedded in ionic media with absorption and magnetic properties determined by size, shape, and composition.[40]Some colloids are found after high doses of irradiation (or severe dose rate) while others require extra annealing to promote diffusion of mobile F-centers. If the heating continues close to melting temperatures, eventually metallic particles will corrode through recombination reactions. Therefore, the colloids represent the ultimate state of F-center aggregation, equivalent to polyhalide association for trapped holes.

CONCLUSIONS

The use of stringent purification techniques and the high sensitivity reached by EPR, and diffuse reflectance optical absorption spectroscopy have enabled characterization of the behavior of KCl-$MgCl_2$ salt mixtures under ionizing radiation fields. It is well known that due to its second ionization potential (I = 15.03 eV), Mg^{2+} is in the intermediate region between divalent cations that are easily radiolytically reduced and those that only generate disturbances in F-centers, becoming monovalent only after thermal treatment. The results presented here confirm that Mg^{2+} belongs to the first group (i.e., easily reduced divalent cations), as changes in Mg^{2+} oxidation state were observed after the dose dependent trapping 1 to 2 electrons in conjunction with the formation of perturbed F-centers. At low Mg^{2+} concentrations (2 mol%), where the Mg^{2+} is well distributed, metal aggregation is reduced, and monatomic species predominate (Mg^{+} and Mg^{0}). Aggregation is enhanced through heating, which also leads to Cl_3^- disproportionation (>400 K). In Mg^{2+} salts with large-size dopants (such as K^{+}), there is an increase in the lattice parameters that facilitates the formation of Mg aggregates. Further, speciation is more varied, including Mg_2, Mg^{0}, Mg^{+}, Mg_3,

and a new center that has not been reported previously, with rhombic symmetry that apparently involves a shared electron between three Mg^{2+} ions (Mg_3^{5+}). Under these conditions, the cluster is paramagnetic and correlates with a band in the visible region (473 nm). Additionally, the presence of Mg and its different oxidation states were found to be in redox equilibrium, reducing the recombination between 300–390 K. All the above indicate how decisive small quantities of Mg^{2+} are in the radiation chemistry of KCl salts, and likely other monovalent chlorides. The fundamental knowledge provided for the present work, will help in the understanding of the ionizing radiation interaction with doped alkali halides crystals, the induced primary long-lived transients, and possible associations in the early stages.

ACKNOWLEDGMENTS

This work was supported as part of the Molten Salts in Extreme Environments Energy Frontier Research Center (MSEE), funded by the U.S. Department of Energy (DOE), Office of Science, Office of Basic Energy Sciences (BES). BNL and INL are operated under DOE contracts DE-SC0012704 and DE-AC07-05ID14517, respectively. MSEE work at the University of Notre Dame is funded under subcontract to Brookhaven National Laboratory. The authors thank Kunal Mondal at INL for performing XRD measurements. The authors thank Prof. Ian Carmichael for making available the facilities of the Notre Dame Radiation Laboratory, which is supported by DOE BES through grant number DE-FC02-04ER15533. This contribution is NDRL-5351 from the Notre Dame Radiation Laboratory.

SUPPORTING INFORMATION

Powder X-ray diffraction spectra for KCl, $MgCl_2$, and KCl:$MgCl_2$ mixtures. EPR spectra of pure KCl irradiated up to 100 kGy. UV-Vis spectra of 98:2 mol%, 2:98 mol%, and 68:32 mol% thermal annealed KCl:$MgCl_2$. EPR spectra of KCl:$MgCl_2$ eutectic mixture.

REFERENCES

1. Grimes, W. R., Molten-Salt Reactor Chemistry. *Nuclear Applications & Technology* **1970**, *8*, 137-155.
2. Lu, J.; Yang, S.; Rong, Z.; Pan, G.; Ding, J.; Liu, S.; Wei, X.; Wang, W., Thermal Properties of KCl–$MgCl_2$ Eutectic Salt for High-Temperature Heat Transfer and Thermal Storage System. *Sol Energ Mat Sol C* **2021**, *228*, 111130.
3. McMurray, J. W.; Raiman, S. S., Thermodynamic Modeling of the K-KCl and Mg-$MgCl_2$ Binary Systems Using the Calphad Method. *Solar Energy* **2018**, *170*, 1039-1042.
4. Xu, X.; Wang, X.; Li, P.; Li, Y.; Hao, Q.; Xiao, B.; Elsentriecy, H.; Gervasio, D., Experimental Test of Properties of KCl–$MgCl_2$ Eutectic Molten Salt for Heat Transfer and Thermal Storage Fluid in Concentrated Solar Power Systems. *Journal of Solar Energy Engineering* **2018**, *140*.
5. Neil, D. E.; Clark, H. M.; Wiswall, R. H., Thermodynamic Properties of Molten Solutions of $MgCl_2$-KCl, $MgCl_2$-NaCl, and $MgCl_2$-KCl-NaCl. *Journal of Chemical & Engineering Data* **1965**, *10*, 21-24.
6. Pikaev, A. K.; Makarov, I. E.; Zhukova, T. N., Solvated Electron in Irradiated Melts of Alkaline Halides. *Radiat Phys Chem* **1982**, *19*, 377-387.
7. Janz, G. J., Physical Properties and Structure of Molten Salts. *Journal of Chemical Education* **1962**, *39*, 59.
8. Wu, F.; Sharma, S.; Roy, S.; Halstenberg, P.; Gallington, L. C.; Mahurin, S. M.; Dai, S.; Bryantsev, V. S.; Ivanov, A. S.; Margulis, C. J., Temperature Dependence of Short and Intermediate Range Order in Molten $MgCl_2$ and Its Mixture with KCl. *The Journal of Physical Chemistry B* **2020**, *124*, 2892-2899.
9. Chiesa, M.; Giamello, E., Electron Paramagnetic Resonance of Charge Carriers in Solids. In *Electron Paramagnetic Resonance. A Practitioner's Toolkit*, Brustolon, M.; Giamello, E., Eds. John Wiley & Sons, Inc: USA, 2009; pp 489-510.
10. Radhakrishna, S.; Chowdari, B. V. R., Z Centres in Impurity-Doped Alkali Halides. *Physica Status Solidi (a)* **1972**, *14*, 11-39.
11. Sootha, G. D.; Singh, D., Optical, Electrical, and ESR Studies of Additively Colored KCl Doped with Magnesium. *Phys Rev* **1969**, *183*, 842-845.

12. Watterich, A.; Raksányi, K., Optical and ESR Investigations of Mg Centres in X-Irradiated and F-Bleached KCl Crystals at RT. *physica status solidi (b)* **1977**, *80*, K105-K108.
13. Damm, J. Z.; Opyrchal, H.; Voszka, R.; Watterich, A., Influence of Mg^{2+} Impurity Ions on the Radiation-Induced for Mation of Colour Centres in KCl Crystals. *Bulletin de l'Academie Polonaise des Sciences Serie des Sciences Chimiques* **1977**, *25*, 311-317.
14. Ramos-Ballesteros, A.; Gakhar, R.; Horne, G. P.; Iwamatsu, K.; Wishart, J. F.; Pimblott, S. M.; LaVerne, J. A., Gamma Radiation-Induced Defects in KCl, $MgCl_2$, and $ZnCl_2$ Salts at Room Temperature. *Physical Chemistry Chemical Physics* **2021**, *23*, 10384-10394.
15. Liu, X., et al., Formation of Three-Dimensional Bicontinuous Structures Via Molten Salt Dealloying Studied in Real-Time by in Situ Synchrotron X-Ray Nano-Tomography. *Nature Communications* **2021**, *12*, 3441.
16. Fricke, H.; Hart, E. J., The Oxidation of Fe++ to Fe+++ by the Irradiation with X-Rays of Solutions of Ferrous Sulfate in Sulfuric Acid. *J Chem Phys* **1935**, *3*, 60-61.
17. Myrick, M. L.; Simcock, M. N.; Baranowski, M.; Brooke, H.; Morgan, S. L.; McCutcheon, J. N., The Kubelka-Munk Diffuse Reflectance Formula Revisited. *Appl Spectrosc Rev* **2011**, *46*, 140-165.
18. Boas, J. F.; Clark, M. J.; Pilbrow, J. R., Epr Evidence for Mg^{+} Ions in CaO. *J Phys C Solid State* **1976**, *9*, 4053-4056.
19. Knight Jr, L. B.; Cleveland, C. B.; Frey, R. F.; Davidson, E. R., Electron Spin Resonance Investigation of Small Magnesium Cluster Cation Radicals, Mg_n^{+}, in Neon and Argon Matrices at 4 K: Comparison with Ab Initio Calculations. *The Journal of Chemical Physics* **1994**, *100*, 7867-7874.
20. Edmonds, R. N.; Harrison, M. R.; Edwards, P. P., Chapter 9. Conduction Electron Spin Resonance in Metallic Systems. *Annual Reports Section "C" (Physical Chemistry)* **1985**, *82*, 265-308.
21. García Solá, J.; Bausá, L. E.; Jaqué, D., *An Introduction to the Optical Spectroscopy of Inorganic Solids*, 1 ed.; John Wiley & Sons, 2005, p i-xx.
22. Mikhailov, M. M.; Ardyshev, V. M.; Belyakov, M. V., Oscillator Strength of Electron-Type Color Centers in KCl Single Crystals Irradiated with Electrons and Protons. *Phys Solid State+* **2002**, *44*, 274-277.
23. Damm, J. Z.; Stepień-Damm, J., Effect of Γ-Irradiation on the Lattice Parameter and Colour Centre Concentration in Pure Ca^{2+}, Sr^{2+} and Eu^{2+} Doped KCl Crystals. *Kristall und Technik* **1980**, *15*, 1167-1172.
24. Bhuniya, R. C., First Stage F Centre Formation in Pure and Doped KCl Crystals by Room Temperaure X-Irradiation. *Czechoslovak Journal of Physics B* **1978**, *28*, 798-806.
25. McCaffrey, J. G.; Ozin, G. A., Photophysical Properties of Matrix-Isolated Mg_2: Evidence for Efficient Predissociation. *The Journal of Chemical Physics* **1988**, *88*, 2962-2971.
26. Voszka, R.; Watterich, A., Experimental Study of a New Mg Centre in NaCl and KCl. *physica status solidi (b)* **1973**, *55*, 787-792.
27. Partin, D. E.; Okeeffe, M., The Structures and Crystal-Chemistry of Magnesium-Chloride and Cadmium Chloride. *J Solid State Chem* **1991**, *95*, 176-183.
28. Shunkeyev, K.; Aimaganbetova, Z.; Myasnikova, L.; Maratova, A.; Ubaev, Z., Mechanisms of Radiation Defect Formation in KCl Crystals under the Influence of Local and Plastic Deformation. *Nuclear Instruments and Methods in Physics Research Section B: Beam Interactions with Materials and Atoms* **2021**, *509*, 7-11.

29. Lushchik, C. B., Creation of Frenkel Defect Pairs by Excitons in Alkali Halides. In *Modern Problems in Condensed Matter Sciences*, Johnson, R. A.; Orlov, A. N., Eds. Elsevier: 1986; Vol. 13, pp 473-525.
30. Shamovsky, L. M.; Rybakova, L. M., Intercrystalline Films in Single Crystals of Alkali Halide Salts and Some of Their Properties. *Doklady Akademii Nauk SSSR* **1953**, *92*, 939-942.
31. Jain, U.; Lidiard, A. B., The Growth of Colloidal Centres in Irradiated Alkali Halides. *The Philosophical Magazine: A Journal of Theoretical Experimental and Applied Physics* **1977**, *35*, 245-259.
32. Ramos B, S.; Hernández A, J.; Murrieta S, H.; Rubio O, J.; Jaque, F., Model for F-Center Production in Alkali Halides Doped with Divalent Cation Impurities That Change Their Valence State by Irradiation. *Phys Rev B* **1985**, *31*, 8164-8170.
33. Gibbons, C. S.; Reinsborough, V. C.; Whitla, W. A., Crystal Structures of K2mgcl4 and Cs2mgcl4. *Canadian Journal of Chemistry* **1975**, *53*, 114-118.
34. Edmonds, R. N.; Edwards, P. P.; Guy, S. C.; Johnson, D. C., Electron Spin Resonance in Small Particles of Sodium, Potassium, and Rubidium Metals. *The Journal of Physical Chemistry* **1984**, *88*, 3764-3771.
35. Watterich, A.; Voszka, R., The Experimental Study of Mg Centres Stable at RT in X-Irradiated NaCl(Mg) Crystals. *Acta Physica Academiae Scientiarum Hungaricae* **1973**, *33*, 323-334.
36. Gachard, E.; Belloni, J.; Subramanian, M. A., Optical and Epr Spectroscopic Studies of Silver Clusters in Ag,Na-Y Zeolite by Γ-Irradiation. *Journal of Materials Chemistry* **1996**, *6*, 867-870.
37. Sako, S.; Kimura, K., Size Effect in Cesr of Magnesium and Calcium Small Particles. *Surf Sci* **1985**, *156*, 511-515.
38. Bandow, S.; Kimura, K., ESR and CESR Observed in Ultrafine Mg Particles. *Solid State Commun* **1990**, *73*, 167-171.
39. Millet, J. L.; Borel, J. P., G-Factor of Magnesium Particles of Diameter between 10 and 30 Å. *Solid State Commun* **1982**, *43*, 217-220.
40. Ekmanis, Y. A.; Pirogov, F. V.; Shvarts, K. K., The Process of Colloidal Centre Formation in Alkali Halide Crystals During Irradiation. *Radiation Effects* **1983**, *74*, 199-208.
41. Egemberdiev, Z.; Elango, A.; Zazubovich, S., Luminescence Accompanying the Recombination of V_f and F Centres in KCl and KBr Crystals. *physica status solidi (b)* **1980**, *97*, 449-456.

TOC Graphic

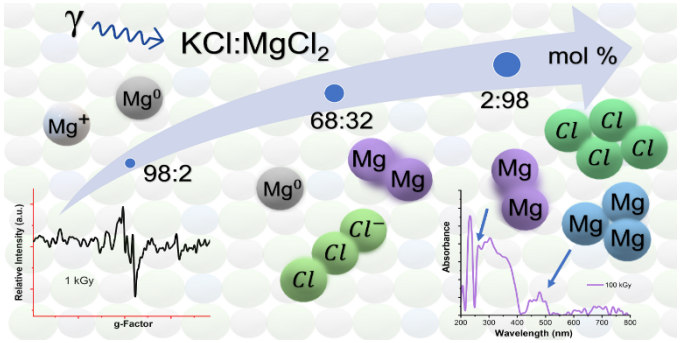
γ
KCl:MgCl2
mol %
Mg0
Mg+
98:2
68:32
2:98
Mg0
Mg
Mg
Cl
Cl
Cl
Cl
Cl
Cl
Mg
Mg
Mg
Mg
Mg
Relative Intensity (a.u.)
1 kGy
g-Factor
Absorbance
100 kGy
200
300
400
500
600
700
800
Wavelength (nm)

SUPPORTING INFORMATION

Radiation-Induced Long-Lived Transients and Metal Particle Formation in Solid KCl-$MgCl_2$ Mixtures

Alejandro Ramos-Ballesteros[1], Ruchi Gakhar[2], Michael E. Woods[2], Gregory P. Horne[3], Kazuhiro Iwamatsu[4], James F. Wishart[4], Simon M. Pimblott[3], and Jay A. LaVerne[1,5].*

[1]Notre Dame Radiation Laboratory, University of Notre Dame, Notre Dame, Indiana 46556

[2]Pyrochemistry and Molten Salt Systems Department, Idaho National Laboratory, Idaho Falls, ID 83415

[3]Center for Radiation Chemistry Research, Idaho National Laboratory, Idaho Falls, ID 83415

[4]Chemistry Division, Brookhaven National Laboratory, Upton, NY 11973

[5]Department of Physics and Astronomy, University of Notre Dame, Notre Dame, Indiana 46556

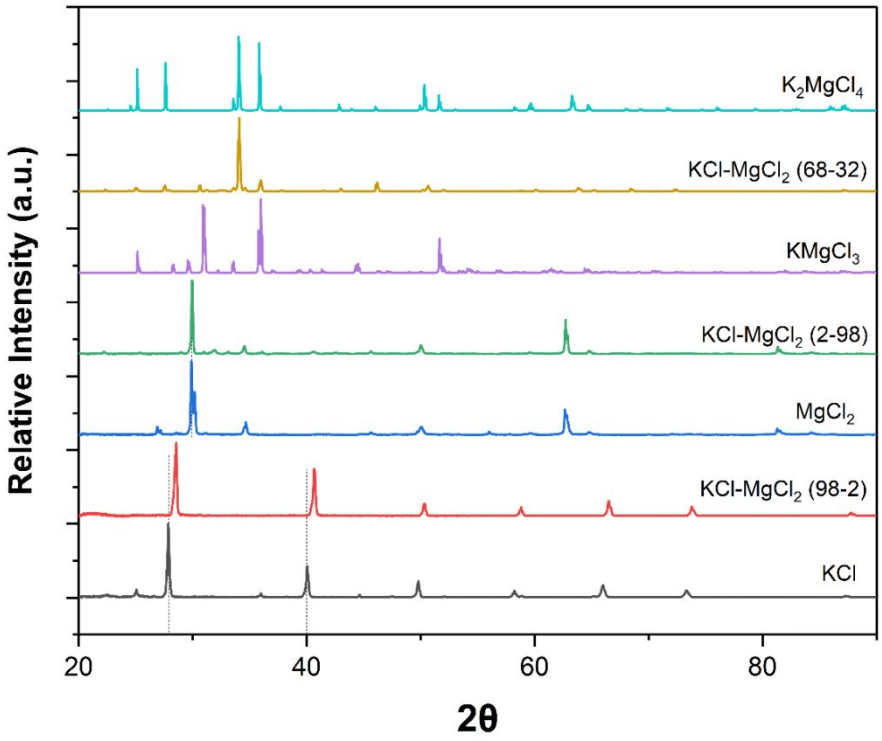

Figure S1. Powder X-ray diffraction spectra for pure halides and mixtures. Theoretical K_2MgCl_4 and $KMgCl_3$ obtained from CIF file (materials project DOI: 10.17188/1201411 and DOI: 10.17188/1202038). Data from Gibbons, C. S., et al. (1975). "Crystal Structures of K_2MgCl_4 and Cs_2MgCl_4." Canadian Journal of Chemistry 53(1): 114-118. Brynestad, J., et al. "Temperature dependence of the absorption spectrum of nickel(II)-doped $KMgCl_3$ and the crystal structure of $KMgCl_3$." Journal of Chemical Physics 45: 4652-4664.

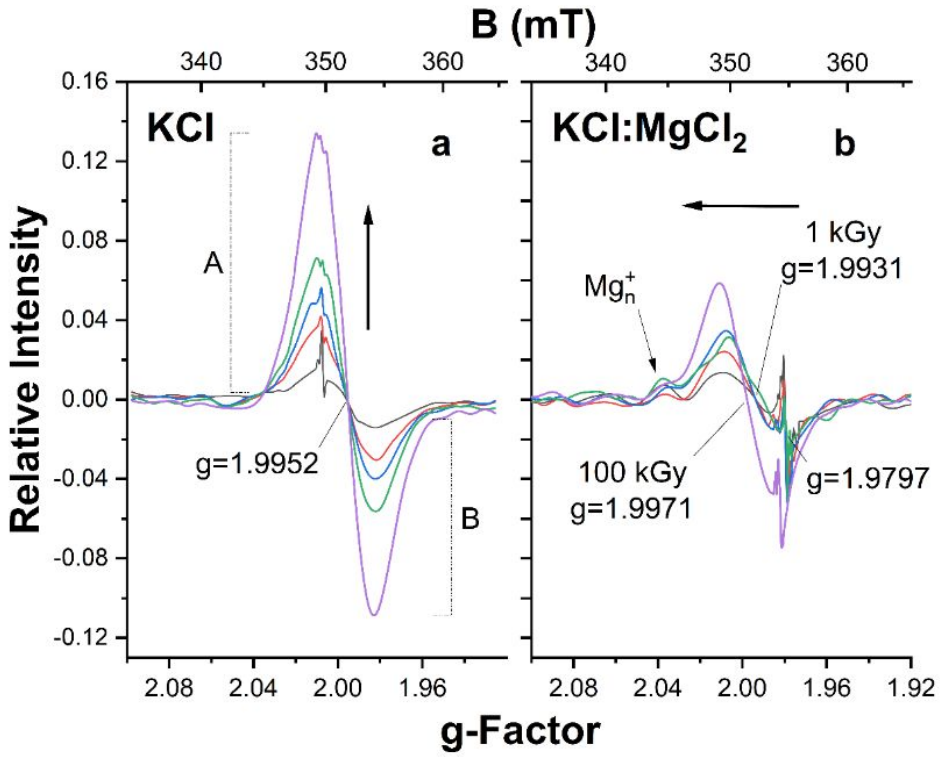

Figure S2. EPR spectra of a) Pure KCl [1] and b) KCl:$MgCl_2$ (98-2 mol%) irradiated up to 100 kGy absorbed dose at 295 K. 1 kGy, 5 kGy, 10 kGy, 20 kGy, and 100 kGy.

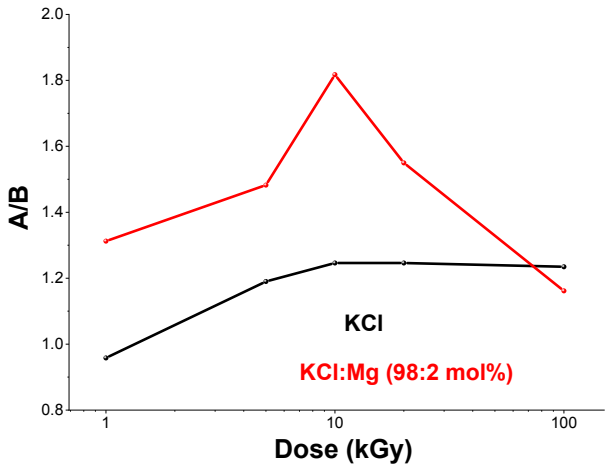

Figure S3. Asymmetry parameter (A/B) of the main resonance EPR line (g=1.99) for pure KCl (black), and 98:2 mol% KCl:$MgCl_2$ (red line) irradiated salts up to 100 kGy.

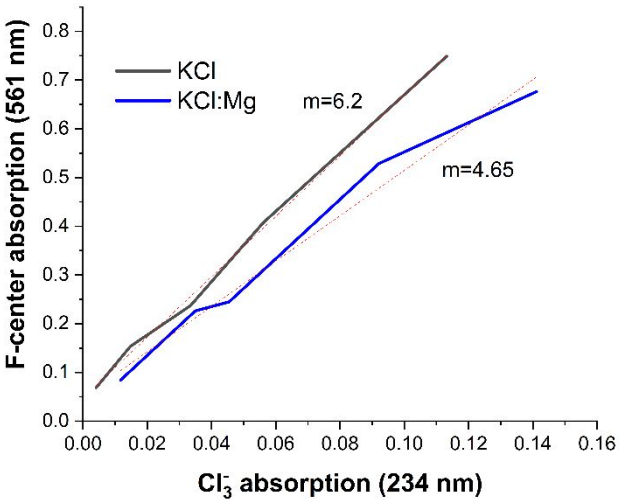

Figure S4. Absorption coefficient ratio F-centers vs Cl_3^- for KCl and KCl:$MgCl_2$ (98-2 mol%).

The change in slope is related to electrons scavenged by Mg.

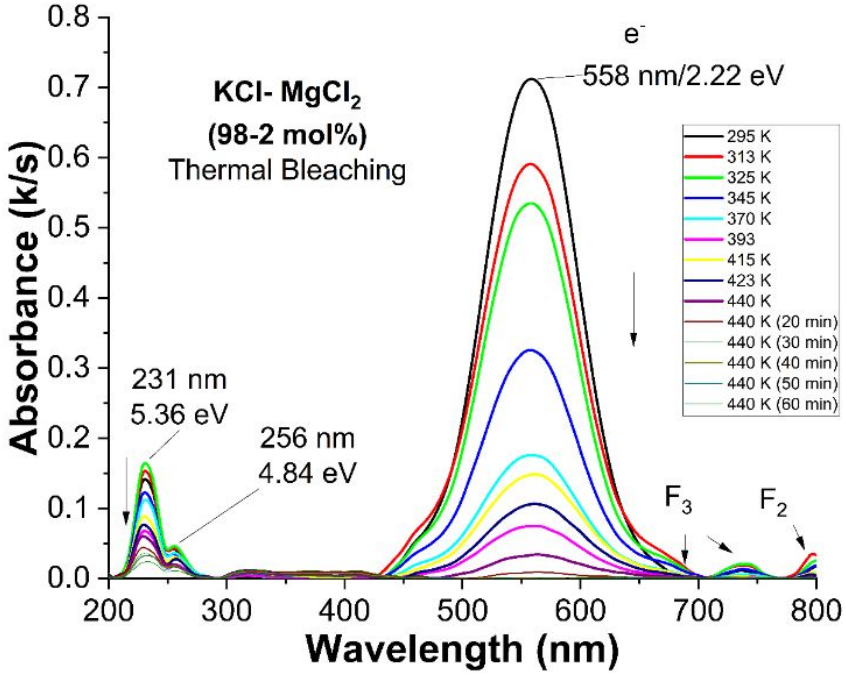

Figure S5. Thermal annealing of irradiated KCl:$MgCl_2$ (2 mol%) powders. Inset shows zoom in for 300-500 nm region corresponding to Mg reduced species.

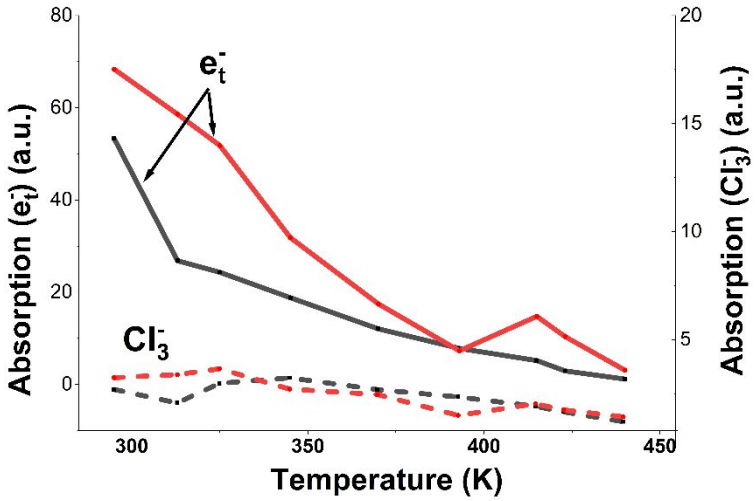

Figure S6. Thermal annealing of e_t^- (solid) and Cl_3^- (dotted) in KCl (black lines) and 98:2 mol% KCl:$MgCl_2$ (red lines) irradiated salts. Absorption calculated from the bands 561 nm for e_t^-, and 234 nm for Cl_3^-.

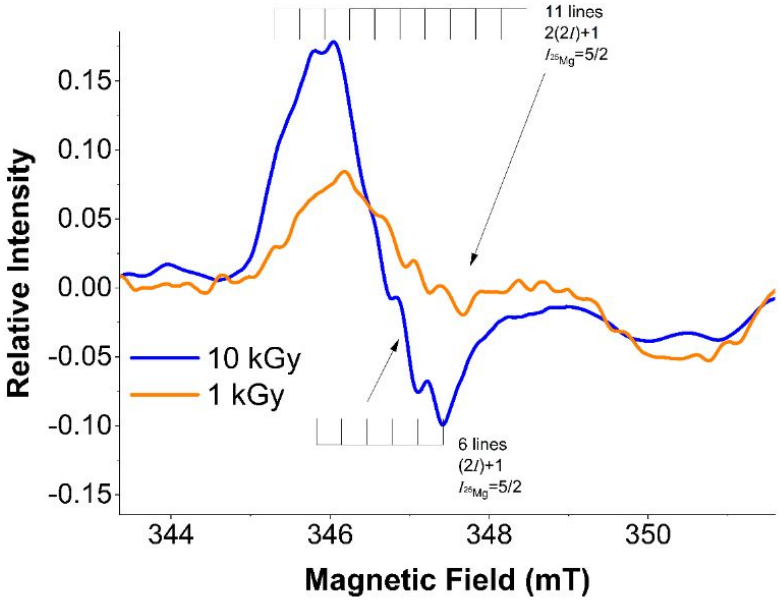

Figure S7. Hyperfine interaction from one and two ^{25}Mg atoms in Mg_3^{5+} for KCl:$MgCl_2$ (2-98 mol%) after 1 and 10 kGy absorbed dose.

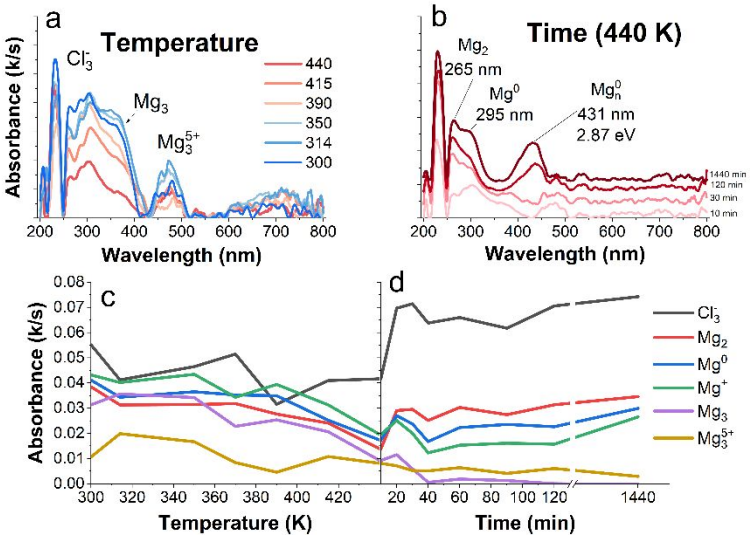

Figure S8. Absorption spectra and thermal annealing curves for different temperatures (a & c) and increasing time at the maximum temperature (b & d).

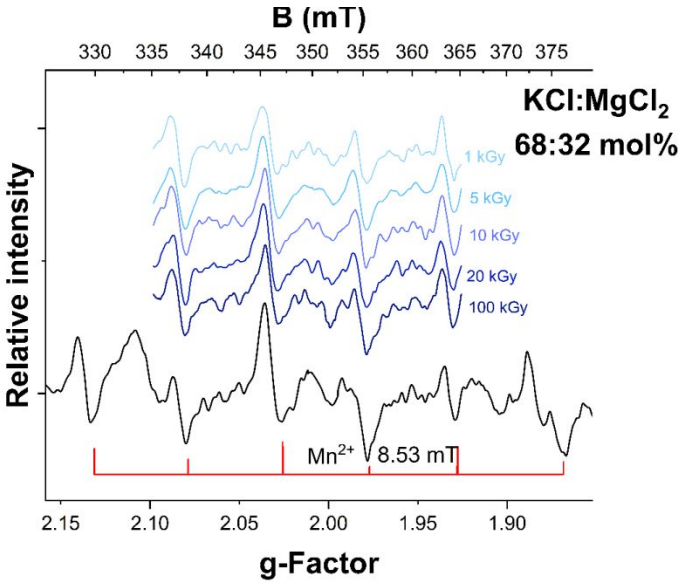

Figure S9. EPR spectra for KCl:$MgCl_2$ eutectic mixture irradiated up to 100 kGy absorbed dose at 295 K. Bottom spectrum corresponds to sample annealed for 24 hr at 440 K after irradiation cycle.

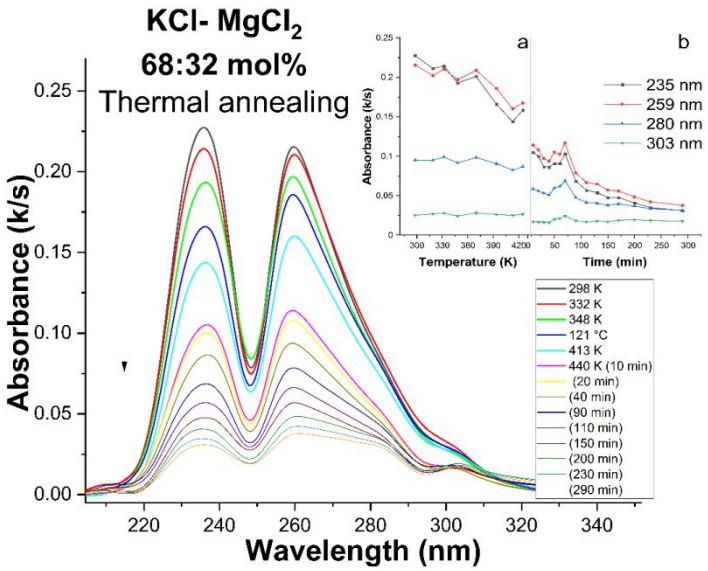

Figure S10. Thermal annealing curves for KCl:$MgCl_2$ eutectic salts irradiated up to 100 kGy at room temperature. The inset shows the decay curves for the 3 main components Cl_3^-, Mg^0 and Mg_2.

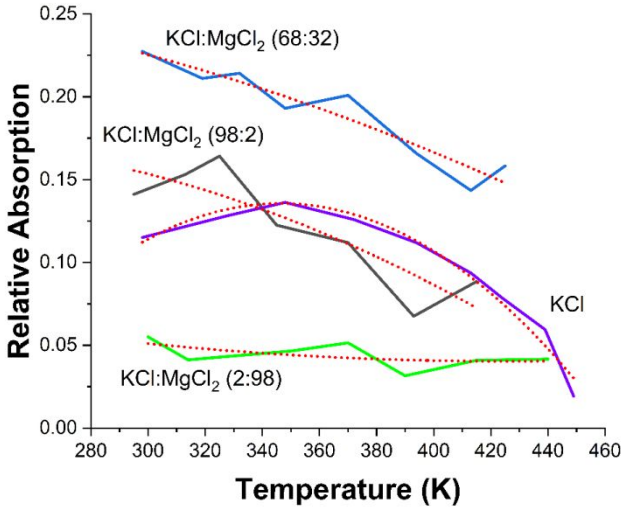

Figure S11. Cl_3^- disproportionation as function of temperature for KCl:$MgCl_2$ (98:2 mol%), KCl:$MgCl_2$ (2:98 mol%), KCl:$MgCl_2$ (eutectic) and pure KCl up to 440 K. Dotted red curves represent quadratic fit.

References

(1) Ramos-Ballesteros, A.; Gakhar, R.; Horne, G. P.; Iwamatsu, K.; Wishart, J. F.; Pimblott, S. M.; LaVerne, J. A. Gamma radiation-induced defects in KCl, $MgCl_2$, and $ZnCl_2$ salts at room temperature. *Phys. Chem. Chem. Phys.* **2021**, *23* (17), 10384-10394, 10.1039/D1CP00520K. DOI: 10.1039/D1CP00520K.